Published in final edited form as:
Langmuir. 2008 September 16; 24(18): 10265–10272. doi:10.1021/la801466e.

Generic Nitric Oxide (NO) Generating Surface by Immobilizing Organoselenium Species via Layer-by-Layer Assembly

Jun Yang, **Jenna L. Welby**, and **Mark E. Meyerhoff***
Department of Chemistry, University of Michigan, 930 North University Avenue, Ann Arbor, Michigan, 48109-1055

Abstract

A universal nitric oxide (NO) generating surface is assembled via Layer-by-Layer (LbL) deposition of sodium alginate (Alg) and organoselenium modified polyethyleneimine (SePEI) on quartz and polymeric substrates. The immobilized SePEI species is capable of catalytically decomposing S-nitrosothiol species (RSNO) to NO in the presence of thiol reducing agents (e.g., glutathione, cysteine, etc.). The stepwise buildup of the multilayer films is monitored by UV-Vis spectroscopy, SEM and surface contact angle measurements. X-ray photoelectron spectroscopy is used to study the stoichiometry between the polyanion and polycation, and also the presence of Se in the catalytic LbL film. A reductive annealing process is necessary to improve the stability of freshly coated multilayer films via chain rearrangement. Chemiluminescence measurements illustrate the ability of the LbL films to generate NO from S-nitrosoglutathione (GSNO) in the presence of S-glutathione (GSH). Enhanced NO fluxes can be achieved by increasing the number of catalytic (SePEI/Alg) bilayers coated on the substrates. Nitric oxide generation is observed even after prolonged contact with sheep whole blood. Preliminary applications of this LbL on silicone rubber tubings and polyurethane catheters reveal similar NO generation behavior from these biomedical grade polymeric substrates.

1. Introduction

Over the past several decades, cardiovascular medicine has progressed into an era where modern devices such as artificial heart valves, stents, vascular grafts, and cardiopulmonary by-pass circuits, etc. are widely employed in life-saving treatments of many patients. However, use of such devices can also promote adverse host responses, particularly risk of thrombosis.[1–6] Immediately after implantation/blood contact, the surfaces of such devices adsorb plasma proteins, propagating the activation of platelets and coagulation factors, and ending in potential blood clot formation.[7] Over the years, various surface treatments and the design of specific polymeric coatings (to reduce protein adsorption, etc.) have been explored to minimize such thrombotic risk.

Recent research carried out in this laboratory[8–12] and elsewhere[13–20] has demonstrated that local nitric oxide (NO) release from polymeric surfaces can exert a highly effective antithrombotic effect by potently inhibiting platelet adhesion and activation. The NO can be released at the implantation site simply by doping NO donors, such as lipophilic N-

*To whom correspondence should be addressed. mmeyerho@umich.edu..

Supporting Information Available: Quantification of Se content in SePEI dry polymer and resulting LbL; quantification of Se leaching from LbL film; selectivity of RSe catalyst with respect to S-nitrosothiols, nitrite and nitrate; effect of annealing on $(SePEI/Alg)_n$ multilayer as characterized by visual observation, UV-Vis and NOA measurements; stability of annealed LbL; curve fitting of XPS N1s envelope; long term NO generation from LbL film; contact angle of various primed silicone rubber surfaces; and UV-Vis study of $(SePEI/Alg)_n$ deposition on primed silicone rubber. This material is available free of charge via the Internet at http://pubs.acs.org.

diazeniumdiolates, into a polymeric matrix,[9, 21–23] or covalently attaching such species to the polymer backbone.[24–29] A continuous NO flux from the surface coating is initiated upon water uptake by the polymer. However, the release rate of NO decreases over time due to depletion of the NO donor reservoir. Recently, several organoselenium species have been shown capable of decomposing endogenous S-nitrosothiols (RSNO) such as S-nitrosoglutathione (GSNO), S-nitrosocysteine (CysNO), etc., to NO in presence of free thiols as reducing agents.[30] Further studies have revealed that these type of catalysts are highly selective for reduction of S-nitrosothiol and exhibit no catalytica activity for nitrite or nitrate reduction (Figure S1 in the Supporting Information). The proposed mechanism comprises a fast denitrosation of RSNO by diselenide (Scheme 1, eq. 4), and a slower catalytic cycle involving a selenolate intermediate which is regenerated by the reducing agent (Scheme 1, eq. 1–3). The potential advantage of applying NO generation to device coatings is that a sustained NO flux can be achieved because the endogenous RSNO level at the implantation site is constantly maintained by blood circulation.

Due to its short lifetime, NO must be generated within close proximity of the surface of any implanted biomedical device to exhibit physiological activity. Confinement of the catalyst on the device surface is therefore required to realize this localized and prolonged NO generation from endogenous RSNOs. Hence, proper immobilization of the catalyst plays a critical role in adapting the aforementioned RSe chemistry into a practical surface NO generation method. Most conventional surface modification methods involve covalently attaching molecules, including catalytic sites, on the substrate surface via a chemical reaction. In this case, both the molecule and the device surface must be properly functionalized. Although various RSe derivatives are available for direct coupling, complicated processing is usually required on the device to provide surface functionality needed for covalent bond formation, especially when the devices are made of chemically inert materials. For example, cellulose filter paper was first oxidized by periodate to generate dialdehyde groups so that selenocystamine could be subsequently immobilized.[30] Recently, a carboxylic acid terminated RSe species was covalently linked to polyethyleneimine (PEI) which was then crosslinked into a hydrogel film within the pore structure of a cellulose dialysis membrane to prepare an amperometric S-nitrosothiol sensor.[31] However, most modern biomedical devices in use do not possess the necessary surface functionality, porosity, and geometric form to enable convenient covalent attachment of the RSe species. Hence, a simple and universal immobilization method feasible to various types of surfaces is needed.

Layer-by-Layer assembly (LbL) has recently emerged as a popular surface modification method.[32–35] A hierarchy multilayer structure is constructed upon exposing a charge bearing substrate alternately into solutions containing anionic and cationic polyelectrolytes. The surface assembly relies on the electrostatic attraction of polyions onto the substrate and the subsequent surface charge reversal. The driving force is purely physical and nonspecific, which allows the realization of this method onto substrates with net surface charge regardless of their nature and topology. This method can also be adapted to surfaces free of charge (mostly polymeric), although a pretreatment is typically required to introduce ionizable functionality to initialize LbL deposition. Methods to prime neutral substrates have been reported utilizing a specific chemical reaction[36–39] or a more universal means such as plasma pretreatment[40, 41] as well as pre-adsorption of some charged polymers on the surface via hydrophobic interaction[42–44]. Over the past two decades, LbL assemblies have been constructed on metal,[45–47] polymer,[36–43] and even biological surfaces.[48] Despite this substrate variety, the properties of an LbL assembly are widely believed to be determined primarily by the nature of the polyelectrolytes employed[49] making this method a truly “generic” surface modification approach. Furthermore, the straightforward dip-wash processing in aqueous solution is more economical, environmentally benign and feasible for automation.

Herein, we report the fabrication and characterization of an LbL assembly possessing immobilized RSe moieties which are capable of generating NO from RSNOs via catalytically decomposing these endogenous NO carriers. The RSe species are immobilized onto cationic PEI and subsequently constructed into the multilayer with sodium alginate as the counter polyanion. The application of this RSe immobilized LbL is examined on various materials, including quartz, silicone rubber, and polyurethane surfaces.

2. Experimental Section

2.1. Materials

Polyethyleneimine (PEI, Mw 25 kD), polydiallyldimethylammonium chloride (PDDA, Mw 100–200 kD), sodium alginate (Alg, Mw 12–80 kD) (Figure 1(b)), glutathione (GSH), fluorescein-5-isothiocyanate (FITC), sodium borohydride ($NaBH_4$), 1-(3-diethylaminopropyl)-3-ethylcarbodiimide (EDC), N-hydroxysuccinimide (NHS), 2-(N-Morpholino)ethanesulfonic acid (MES), and 2-(N-cyclohexylamino)-ethanesulfonic acid (CHES) were obtained from Sigma-Aldrich (St. Louis, MO). The 3140 RTV Silicone Rubber was purchased from Dow Corning Corporation (Midland, MI). All reagents were used as received except for alginate, a solution of which was first membrane filtered (Durapore® 0.1 μM, Millipore Corp. (Billerica, MA)) to remove insoluble impurities before use. 3,3'-Diselenidedipropionic acid (SeDPA) and S-nitrosoglutathione (GSNO) were synthesized as described previously.[30] All solutions were prepared with 18 MΩ cm^{-1} deionized distilled water obtained from a Milli-Q system (Millipore Corp., Billerica, MA).

2.2. Preparation of Organoselenium Immobilized Polyelectrolyte (SePEI)

To integrate catalytic activity into an LbL structure, a small molecule organoselenium species, SeDPA, must be covalently linked to a polycation or polyanion without significantly compromising the capability of the polyelectrolyte to interact with its oppositely charged counterpart. Polyethyleneimine was selected due to the abundance of primary amines within its structure which can be reacted readily with activated carboxylic acid group. SePEI (Figure 1(a)) was synthesized following a procedure slightly modified from the one reported earlier.[30] SeDPA (76 mg, 0.25 mmol) was activated with EDC (285 mg, 1.5 mmol) and NHS (115 mg, 1 mmol) and the reaction mixture was allowed to react with PEI (20 mg) in MES buffer (pH = 6.0) for 2 h. The resulting SePEI was separated by centrifuging the mixture in an Amicon® centrifugal filter unit (MWCO = 3 kD, Millipore Corp., Billerica, MA) at 4,000 rpm for 40 min. Although SeDPA has two carboxylate groups capable of reacting with PEI, sometimes only one of the two carboxylic acids forms the desired amide bond during EDC/NHS coupling, leaving an unreacted half molecule attached to the polymer through only a diselenide bond with the reacted half. When the diselenide bond is reduced by GSNO or GSH, the unreacted half molecule will be liberated and cause serious leaching. Hence, the SePEI was initially reduced with $NaBH_4$ to break any diselenide crosslinks into selenols and then exhaustively dialyzed (Spectra/Por® 7, MWCO = 3.5 kD, Spectrum Laboratories Inc., Rancho Dominguez, CA) in 50 mM NaCl for 3 days to remove any unreacted -SeC_2H_4COOH halves. The dialyzed solution was then further concentrated into a yellow viscous solution and stored at 4 °C till use. The yellow color indicates the reformation of diselenide bonds between PEI chains due to oxidation of selenols by ambient O_2 during dialysis. Nevertheless, the crosslinked SePEI still exhibits good solubility in water as suggested by the absence of any precipitation. The Se content in the SePEI polymer was quantified using ICP-MS to be 6.6 ± 0.1 *wt* % (0.85 ± 0.01 mmole g^{-1}) of dry polymer (Table S1 in the Supporting Information).

2.3. Labeling of SePEI with FITC Chromophore

Despite of its characteristic absorbance in near UV region, the diselenides present in the LbL coating are not easily observed due to their low quantity and low molar extinction coefficient

(ε_{300} = 240 M^{-1} cm^{-1})[50]. Therefore, the SePEI polymer was labeled with FITC chromophore (ε_{495} = 76,000 M^{-1} cm^{-1})[51] to render the polymer spectroscopically visible. SePEI in CHES (2 mg mL^{-1}, 10 mL) was mixed with FITC/DMF solution (1 mg mL^{-1}, 0.8 mL) under constant stirring for 1 h. The resulting orange adduct was washed, concentrated and redissolved in PBS for subsequent use. The labeling degree was calculated to be 0.53 using protocol provided by Sigma Aldrich.[52] This labeled SePEI was exclusively employed for all UV-Vis studies to observe stepwise deposition of SePEI during the LbL process.

2.4. Construction of NO Generating Layer-by-Layer Films on Quartz Surfaces

All polyelectrolytes were prepared as 1 mg mL^{-1} solutions: PDDA was dissolved in CHES (pH = 9.3), while SePEI and Alg were made in PBS (pH = 7.4). The quartz substrate (either slide or cuvette) was cleaned in piranha solution (3:7 v/v H_2SO_4/H_2O_2 mixture) for 30 min before use to fully remove surface impurities. *(Caution: this solution is extremely corrosive.)* The LbL multilayer was then prepared by immersing the substrate alternately into the polycation (SePEI or PDDA) and polyanion (Alg) solutions for 10 min with washing with PBS buffer after each deposition step. Briefly, a $(PDDA/Alg)_2$ film was coated as a precursor layer to stabilize and amplify the surface charge on the substrate. Then, SePEI and Alg were deposited alternately until a desired number of (SePEI/Alg) bilayers were reached. A reductive annealing process follows the step-by-step deposition to further stabilize the polyelectrolyte structure. The freshly prepared LbL was immersed in a 20 mL disposable scintillation vial filled with 100 μM GSH in PBS. The setup was wrapped with aluminum foil and kept at room temperature overnight before the catalytic activity of the resulting LbL was examined.

2.5. Characterizations of $(SePEI/Alg)_n$ on Quartz Substrate

2.5.1. UV-Vis—The stepwise growth of the LbL film was monitored using a UV-Vis spectrophotometer (Lambda 35, Perkin Elmer, MA). The LbL was constructed on the inner wall of a quartz cuvette by filling the cuvette with polyelectrolyte solutions in the sequence described above. The cuvette was then scanned from 550 nm to 450 nm with a data interval of 1 nm after every (SePEI/Alg) bilayer was deposited. The FITC labeled SePEI species was employed exclusively in this study.

2.5.2. XPS—X-ray photoelectron spectroscopy was performed on a Kratos Axis Ultra XPS (Kratos Analytical, England). The X-ray source employed was a monochromatized Mg Kα operated at 10 kV/ 80 W with pass energy of 80 eV. Charge neutralization was used to compensate the charge accumulation on the sample. The coating was scanned at step sizes of 1 eV and 0.1 eV (0.1 s each step) for survey and core scans, respectively. Prior to the measurement, the sample was out-gassed overnight in the sample transfer chamber under high vacuum. The spectrum was processed using CasaXPS version 2.3.12.

2.5.3. SEM—Surface morphology of the polyelectrolyte multilayers was examined on a FEI Nova Nanolab Scanning Electron Microscope via the detection of secondary electrons. The specimens were dried in a N_2 atmosphere overnight and then gold coated using a SPI Sputter Coater at 18 mA for 60 s for better imaging.

2.5.4. Contact Angle—Static air–water contact angles were measured by a sessile drop method using a Cam-100 Optical Contact Angle Goniometer (KSV Instruments Ltd., Monroe, CT) at ambient humidity and temperature. The annealed LbL coated on glass slides were dried with N_2 flow for 2 d. For each polymer surface, 4 drops were examined to obtain the average contact angle values.

2.5.5. NO Detection—Slides coated with $(SePEI/Alg)_n$ LbL films were inserted into a PBS (2 mL, pH = 7.4) test solution containing GSNO and GSH. The coating area that was submerged

by the test solution and therefore involved in the catalytic reaction was ca. 3 cm^2. The NO produced was purged from the solution with N_2 flow and detected using a chemiluminescence NO analyzer (NOA) (Seivers 280, Boulder, CO). The amount of NO evolved from the solution was calculated based on the calibration curves of the NOA, which were obtained regularly by plotting the integrated NOA signal (ppb s) during calibration vs. the introduced amount (moles) of NO into the system via nitrite reduction in an acidified potassium iodide solution. To prevent unwanted RSNO decomposition from external thermal or photo stimuli,[53] all NOA tests were performed at room temperature using amber reaction vessels. Lights in the laboratory were also turned off when these experiments were conducted. EDTA was added to the testing solution in order to eliminate any GSNO decomposition catalyzed by trace metal ions, e.g. Cu (II).

2.5.6. *In Vitro* Blood Test—Fresh heparinized (5 U mL^{-1}) sheep whole blood was obtained from ECMO Laboratory in the Medical School at the University of Michigan. 3 mL of blood was carefully transferred into a 15 mL polypropylene centrifuge tube. A glass slide coated with $(SePEI/Alg)_{10}$ was gently positioned in the blood. The tube was sealed and wrapped with aluminum foil to reduce light exposure. During the entire procedure, the blood surface was kept below the top of the coating to avoid any accidental contact with bare glass. After 24 h incubation at 4 °C in the dark, the slide was removed and rinsed with PBS buffer to wash off any loosely adsorbed blood residue. A control slide was immersed in 3 ml PBS and processed following the same procedure. The ability of the resulting LbL to generate NO from GSNO was then examined by the chemiluminescence method described above.

2.5.7. Quantification of Se in $(SePEI/Alg)_{10}$—A slide (1 × 2 cm) coated with 10 (SePEI/Alg) bilayers was placed in a vial containing 4 mL 100% fuming nitric acid. The polyelectrolyte film immediately peels off from the slide upon acidification and floats freely in the acid. The vial was capped and kept at room temperature for 24 h during which the LbL broke down into a number of small pieces. Then, the acid was heated up to 60 °C until all these small pieces were completely digested. The digesting solution was brought to a volume of 25 mL using a volumetric flask and sent for ICP-MS quantification of Se content. Another vial containing same amount of nitric acid but without the multilayer was also prepared following the same protocol and was used as control.

2.5.8. Se Leaching Test—$(SePEI/Alg)_{10}$ was coated on glass shell vials (1.5 cm ID, 3.5 cm, Fischerbrand®, Fischer Scientific Inc., Pittsburgh, PA). The coating area was calculated to be 12.4 cm^2. Four mL of PBS buffer containing 100 μM GSH and 50 μM GSNO was added to each vial, which is enough to submerge the entire coating area, to extract leachable selenium species from the LbLs. The vials were then capped, wrapped with aluminum foil, and kept at room temperature for 5 d. Every 24 h, the extracting solutions were collected and the vials were refilled with fresh PBS buffer containing the same concentration of GSH and GSNO. After a 5 day extraction period, the LbLs were digested using nitric acid (see Section 2.5.7) to quantify the remaining Se in the coatings. The extracts and digesting solutions were brought up to a volume of 25 mL for subsequent ICP-MS measurements.

2.6. Polymeric Substrates Preparation

Silicone tubing (0.64 mm ID/1.19 mm OD, 2 cm), purchased from Helix Medical Inc. (Carpinteria, CA), and 5 Fr double lumen polyurethane catheter (Cook, Denmark) were cut into 1 inch segments. The open ends of these segments were sealed with RTV 3140 SR followed by curing under ambient conditions overnight. Before immersion in polyelectrolyte solutions for LbL deposition, the polymeric substrates were cleaned by sonicating in deionized H_2O and ethanol for 20 min each. The silicone rubber was soaked in PBS overnight before placing into

a PDDA solution, whereas the polyurethane substrate was directly coated with $(SePEI/Alg)_n$ without a precursor layer.

3. Results and Discussion

3.1. Fabrication and Characterization of $(SePEI/Alg)_n$ LbL on Quartz Substrates

The successive adsorption of $(SEPI/Alg)_n$ can be discerned by visually examining the quartz substrates after every immersion in Alg solution. After the 4th cycle, the quartz slide became cloudy and progressively lost its transparency as more bilayers were deposited. The presence and propagation of this cloudiness suggest formation of a heterogeneous film structure which is attributed to the fast adsorption kinetics.[54] Indeed, when the substrate is alternately immersed into SePEI and Alg solutions, the polyions associate at the interface at such a fast rate that many defects are trapped and chain rearrangement does not have sufficient capacity to "heal" the defects in time before another coating cycle. In good agreement with visual observations, UV-Vis spectra of the LbL films exhibit a steady background absorbance increase owing to the heterogeneity of the multilayer. Due to FITC tracer, the $(SePEI/Alg)_n$ displays a maximum absorbance at 503 nm which was extracted and plotted against the number of bilayers in the LbL. As shown in Figure 2, the absorbance displays an ascending trend suggesting that the quantity of SePEI on the substrate increases continuously during the LbL deposition.

Interestingly, the UV-Vis data shown in Figure 2 exhibits an "S" shape rather than a uniformly linear or exponential type curve that is typically observed in LbL assembly.[55–58] The slope of the curve is very flat initially but becomes steeper from the 4th bilayer and then flattens again since the 6th bilayer. Such a variation suggests a possible surface morphology evolution of the LbL, given that the SePEI is electrostatically attracted by the existing multilayer on the substrate. Therefore, SEM snapshots of $(SePEI/Alg)_n$ were taken to assess surface features at various stages of the coating process. The initial $(PDDA/Alg)_2$ precursor layer is found to provide a smooth and even coverage on the quartz substrate (Figure 3a). One (SePEI/Alg) bilayer only slightly roughens the surface with scattered islands that are hardly distinguishable from the background owing to their small dimensions (Figure 3b). When more layers of the polyelectrolytes are deposited, the tiny islands quickly develop into coalesced large particles with a maximum diameter of ca. 2 μm, which considerably roughen the surface (Figure 3c–d). This observation supports the same heterogeneous LbL structure implied by the UV-Vis study. In fact, a recent study has reported that LbL coatings do not start growing as a successive superposition of interacting polymer layers, and polyelectrolyte adsorption is kinetically stopped by the surface potential reversal other than at full coverage of the substrate.[59] In our case, the PEI crosslinked by the diselenides possesses a bulkier conformation compared with linear polyelectrolytes, and this further sterically impedes the effective interaction of the SePEI with the substrate. As a result, little adsorption of SePEI results in accumulation of enough positive charge to reverse the surface potential, which explains the slow increase in UV-Vis adsorption for the first couple of coating steps. A full coverage of the surface is finally realized after 4 bilayers (Figure 3e); however, the earlier coarse structure can still be vaguely recognized from the bumpy surface contour. Continuous deposition of polyelectrolytes significantly smoothes the bumpiness and leads to more modest surface irregularities (Figure 3f). The transition from discrete particles to continuous layer as well as the subsequent smoother surface can be attributed to the propensity of polyelectrolytes to bridge over the underlying defects. Based on the SEM data, we speculate that the over adsorption of SePEI from the 4th to 6th bilayer is chiefly a matter of greater surface roughness which increases the surface area. After the 6th bilayer, the growth enters a "self-regulated" regime where the structure and properties of the outer layer converge into a state determined by the nature of the polyelectrolyte pair.[34]

The kinetically ruled layer-by-layer adsorption results in a heterogeneous film structure which is thermodynamically unstable. An annealing process is therefore required to reduce the

existing defects through self-rearrangement of polymer chains. Although the chain mobility in an LbL film is almost completely lost in dry state, it can be regained to a certain degree upon immersion in water.[54] We find that a $(SePEI/Alg)_5$ annealed in PBS containing 100 μM GSH can revert to a film with greater clarity (Figure S2 in the Supporting Information). The annealed LbL retains 92.2% of its original FITC absorbance suggesting that the observed improvement in film clarity is not due to delamination of the multilayer (Figure S3 in the Supporting Information). In contrast, the specimen annealed in PBS without the presence of GSH only partially loses its cloudiness. The presence of GSH likely facilitates the healing process by reducing most of the diselenide crosslinks and yielding SePEI polymers that are smaller in size and more readily rearrange into a more thermodynamically stable conformation. The SEM images (Figure 4) at low magnification clearly show that the fuzzy appearance of freshly coated LbL surface develops into a denser layer embedded with coarse clumps up to 10 μm in diameter after annealing. Such a surface conformational change further verifies the occurrence of chain rearrangement. The annealed $(SePEI/Alg)_n$ multilayer exhibits an improved stability. After 4 d exposure in PBS in presence of 100 μM GSH and 50 μM GSNO, the multilayer preserves 95.3% of its original UV-Vis adsorption (Figure S4 in the Supporting Information). Se content in such annealed $(SePEI/Alg)_n$ LbLs was determined to be ca. 2.9 μg cm^{-2} (0.036 μmole cm^{-2}) for a 10 bilayers structure (Table S2 in the Supporting Information).

The annealed $(SePEI/Alg)_n$ LbLs were also characterized via contact angle. Figure 5 shows the static contact angles of the films at each deposition step with pure water measured in atmospheric air at room temperature. In the early stage, the surfaces exhibit similar contact angles regardless of which polyionic species is the outermost layer. This can be explained by the prevalent occupancy of the surface by the initial $(PDDA/Alg)_2$ precursor layer due to the poor coverage of the $(SePEI/Alg)_n$. From the 3rd coating cycle onward, the contact angles fluctuate periodically between 64.1 ± 3.3 for the SePEI as the outermost layer and 56.7 ± 3.1 for Alg as the outermost layer. This back-and-forth change of surface tension further verifies the LbL buildup of the film by alternate deposition of SePEI and Alg.

The chemical composition of the $(SePEI/Alg)_n$ LbL was also studied using X-ray photoelectron spectroscopy (Figure 6). The peak at 57 eV was identified as Se 3d electron, which confirms the immobilization of organoselenium species within the multilayer. Slight amounts of Cl and P were also found in the film, probably from the $H_2PO_2^-$ and Cl^- small ions in the buffer in which the LbL was deposited. The amine:carboxylate ratio was determined to be 3.89 based on the atomic percentage of N and O. Curve fitting of the N 1s envelope in the core scan indicates that only 27.5% of the SePEI amines are in their ionized cationic form (Figure S5 in the Supporting Information). Such a low ionization degree is expected for branched PEI in which a great amount of secondary and tertiary amines distribute densely on the polymer backbone. Protonation of neighboring amine groups can therefore invoke considerable electrostatic repulsion. Indeed, the pKa values of branched PEI were reported in a recent work to be 9.2, 8.2, 5.8 and 4.3, respectively.[60] We think most of the cationic amines are contributed by the uncoupled primary amines locating at the end of the branches of PEI molecules, which are far away from each other and thus invoke less repulsive interaction upon protonation. If this partial ionization of SePEI is taken into account, the ratio of cationic amines and carboxylates is close to a 1:1 ratio. This explains the appearance of only a trace amount of small counterions in the film, although the total amine is in great excess to the carboxyl groups of the Alg species.

3.2. NO Generation from GSNO Catalyzed by $(SePEI/Alg)_n$ LbL on Quartz Surfaces

The catalytic activity of $(SePEI/Alg)_n$ deposited on quartz slide was investigated by measuring NO generation from GSNO with GSH as reducing agent via chemiluminescence. Figure 7 shows a typical chemiluminescence result obtained from a $(SePEI/Alg)_5$. Nitric oxide

production is initiated instantly upon introducing the slide into the test solution and plateaus at a sustained NO level rapidly. When the slide is removed, the NO generation ceases almost entirely, indicating the catalytic GSNO breakdown occurs predominantly in the LbL film on the slide. Repeated immersion and removal of the slide replicate the up-and-down NO generation pattern. The NO flux degrades slightly over time which is likely attributed to the consumption of the GSNO in the bulk test solution. Although GSNO can directly react with GSH to produce nitroxyl and potentially compete with the catalytic GSNO decomposition employed in our experiments,[61] we believe that the reaction rate for nitroxyl formation is much slower and the RSe catalyst dependent GSNO decomposition is the primary reaction by which GSNO is consumed in the reaction mixture. The marginal baseline increase after slide removal suggests only a very small amount of catalyst leaches from the LbL film into the test solution during the measurements, with no severe delamination of the catalytic multilayer observed. Indeed, the return to baseline in the chemiluminescence experiments after removing the LbL coated substrate is a very sensitive means to probe the degree of leaching, since any loss of RSe species will induce a homogenous reaction which is much faster than the heterogeneous surface reaction mediated by the LbL. Assembly that had not been annealed was also tested. A significant NO generation from bulk solution was observed indicating substantial catalyst leaching from the LbL into the test solution (Figure S6 in the Supporting Information). Such results further confirm the enhanced stability of the LbL assembly that is induced by the annealing step.

It should be recognized that a solid polymer matrix would likely block the free diffusion of the reactive GSNO and GSH species from penetrating into such a coating. If inner RSe catalytic sites are not accessible to GSNO substrate and GSH reducing agent, the amount of NO generation would be solely dictated by reactions at the outer surface of the polyelectrolyte coating but not the number of bilayers within the LbL film. However, if the film is truly permeable to GSNO and GSH, there should be an increase in observed NO production for thicker films. Hence, $(SePEI/Alg)_n$ with various numbers of catalytic bilayers were tested to evaluate the accessibility of the RSe sites within the LbL. Figure 8(a) clearly shows the maximum NO flux increases from 56 ppb for $(SePEI/Alg)_5$ to 106 and 146 ppb for $(SePEI/Alg)_{10}$ and $(SePEI/Alg)_{15}$, respectively. Meanwhile, the background solution phase NO generation (after slide removal) does not show a significant increase for the greater number of bilayers deposited. This proves that the enhanced NO production is indeed derived from the access to the RSe catalyst in the underlying layers of the LbL coating. The correlation between the maximum NO flux observed in NOA studies and UV-Vis adsorption of LbL with various numbers of bilayers is nearly proportional (see Figure 8(b)). Such a result implies a very open film structure in which most of the immobilized RSe species are able to contribute to GSNO breakdown even for films with 15 bilayers. This is an attractive feature of this new NO generating coating in that the degree of NO generation from given RSNO/RSH concentrations can be controlled by the number of bilayers deposited.

In a longer term study, ten separate aliquots of PBS buffer (2 mL in each aliquot) containing the same initial concentrations of GSNO and GSH (50 μM and 100 μM, respectively) were allowed to react successively with a single quartz slide coated with a $(SePEI/Alg)_{10}$. The LbL was kept in each test solution until the NO production fully stopped and subsequently transferred to the next test solution. After continuously reacting for 40 h in total, the LbL still exhibited significant catalytic activity (Figure S7 in the Supporting Information). The conversion rate of GSNO was calculated separately for all 10 reactions revealing that the GSNO in each batch was completely depleted. The estimated Se content in the LbL was 0.11 μMol, while the total GSNO decomposed was 1 μMol. It is obvious that the $(SePEI/Alg)_n$ can consume GSNO effectively and decompose more GSNO than the amount of Se immobilized in the multilayer film, further proving that the reaction is catalytic in nature. The extended reaction time also resulted in a slower kinetics. Compared with the 1st batch, the maximum NO flux in

the 10^{th} experiment decreases about 60%, while the time required to decompose all the GSNO is almost doubled.

The organoselenium immobilized LbL was also tested *in vitro* to preliminarily evaluate its activity after prolonged contact with sheep whole blood (Figure 9). Without spiking additional GSNO, the endogenous GSNO and other RSNO concentrations in the blood decrease rapidly due to the consumption by the catalyst. After 24 h of contact, the LbL was thus partially covered by thrombus (since NO generation ceases without more substrate). When the blood clots were carefully peeled off with tweezers, the LbL underneath still displayed significant catalytic activity in generating NO from a fresh GSNO/GSH solution (Figure 9b) and was able to fully convert all the GSNO added in the reaction. However, the LbL in contact with blood displayed a lower NO generating activity (ca. 50% less) compared with the control (Figure 9a) which had been in contact only with PBS buffer. Several experimental aspects may account for this activity decay. It is possible that part of the multilayer is delaminated simultaneously upon the clot removal and herein reduces the catalyst quantity in the assembly. Protein adsorption on the LbL surface may also slow down diffusion of GSNO/GSH reactants into the coating and thus results in slower reaction kinetics. Nevertheless, the *in vitro* blood contact study strongly suggests that $(SePEI/Alg)_n$ LbL coatings can preserve significant activity after exposure in blood components for an extended time period.

Despite being an essential trace element in the diet, toxicity of selenium has been well recognized and correlated to the oxidation state of selenium.[62] The upper limit of selenium intake for humans from all sources is 400–450 μg per day as recommended by several expert panels.[63–65] To assess potential toxicity risk of such a $(SePEI/Alg)_n$ LbL, a leaching test was performed by extracting leachable RSe species from a $(SePEI/Alg)_{10}$ under reaction condition for 5 d. ICP-MS results reveal only 3.0% Se leach out from the catalytic multilayer after 5 d extraction (Table S2 in the Supporting Information). Notably, the leaching rate is lower than the kinetics decrease that was observed in aforementioned long term study, indicating that some selenium active centers are deactivated but they still remain attached to the polyelectrolyte matrix. Thus far, the exact Se species that leaches from the LbL films has not been identified and the deactivation mechanism remains unclear. We speculate the leaching and deactivation of RSe catalyst is due to the instability of aliphatic organoselenium species. Diselenides can undergo alkaline hydrolysis in basic conditions.[66] Therefore, it is possible that SeDPA is slowly destabilized by the basic local environment created by the PEI amine sites. Also, the anionic selenolate intermediate is a very good nucleophile and a strong reductive species. This species can undergo a lot of unwanted side reactions and easily get oxidized into higher oxidation states by various oxidizing species.[66]

3.3. Application of $(SePEI/Alg)_n$ LbL on Polymeric Surfaces

The primary motivation for this study is the potential application of this RSe immobilized LbL approach to render biomedical materials/devices more biocompatible via spontaneous generation of NO from endogenous blood components. Toward this goal, it is important to demonstrate that the $(SePEI/Alg)_n$ film can be coated on biomedical grade silicone rubber and polyurethane, both are widely used to make biomedical devices. Several methods were examined to create surface charge on silicone rubber, including silanization with 3-aminopropylsilane (APS), adsorption of PDDA, and adsorption of SePEI. All three methods lower the surface contact angle of the silicone rubber by 4–6° (Figure S8 in the Supporting Information). The surface charge of the treated (charged) silicone tubing was reversed by a layer of Alg and further stabilized with $(PDDA/Alg)_2$ before $(SePEI/Alg)_n$ LbL film was assembled. UV-Vis studies reveal little disparity in the stepwise growth of the resulting LbLs, regardless of the various surface charging methods employed (Figure S9 in the Supporting Information). Figure 10(a) shows the NO generation from $(SePEI/Alg)_{10}$ on silicone tubing

upon repeated immersion and removal of the LbL coated tubing into a solution of 50 μM GSNO and 50 μM GSH in PBS buffer. It is clear that the catalytic behavior of the film on silicone rubber is quite similar to that observed on quartz.

The LbL assembly was also applied on the surface of PU-based catheters without a precoating with $(PDDA/Alg)_2$ precursor layers. Indeed, PEI can absorb on polymeric surfaces via hydrophobic interaction to introduce cationic amine groups and initialize LbL growth.[44] As shown in Figure 10(b), the resulting coated device with 10 bilayers exhibits similar catalytic NO generation. In concert with the experiments performed on quartz slides, these results prove that the $(SePEI/Alg)_n$ behaves similarly even when applied on substrates with vastly different initial surface properties. The normalized NO fluxes observed when in contact with a 50 μM GSNO and 50 μM GSH solution are 2.4×10^{-10} and 1.8×10^{-10} mol min^{-1} cm^{-2} for silicone and PU substrates, respectively. These are comparable with the physiological NO levels ($0.5 – 4.0 \times 10^{-10}$ mol min^{-1} cm^{-2}) generated by healthy endothelium cell lining the blood vessels.[25, 67–69] While the NO levels that would be generated when devices are in contact with fresh flowing blood will vary depending on the levels of RSNOs and free thiols (GSH and cysteine), recent studies have shown that NO generating polymer coatings based on copper catalysts, that carry out the same reactions as the RSe used here, do reduce thrombus formation on catheter surfaces when implanted in pig arteries for up to 20 h (compared to controls in the same animals).[11]

4. Conclusion

In summary, a novel strategy to immobilize catalytic organoselenium species via layer-by-layer deposition method has been described. The catalytic multilayer was shown capable of generating NO from GSNO, an endogenous NO precursor, for an extended time period. The surface confined polyelectrolyte matrix exhibits sufficient permeability to GSNO and GSH small molecules to access catalytic sites deep within the structure. Even after prolonged contact with blood, the LbL still preserves significant catalytic activity. Our preliminary studies using silicone rubber and polyurethane substrates clearly demonstrate that this NO generating surface can be easily adapted onto currently commercialized biomedical polymers used for vascular grafts, catheters, etc.

The current LbL NO generating coatings exhibit very low catalyst leaching from the multilayer. Recently, the leachable components of $(SePEI/Alg)_{10}$ have been extracted and tested in mice for systemic toxicity following ISO 10993-11 and ISO 10993-12 procedures. No apparent toxic symptoms have been observed in these preliminary tests. It is also noteworthy that the average daily dietary intake of selenium in the United States is consistently above 55 μg per day and a super-nutritional level (> 100 μg) is suggested to optimize its anti-oxidation potency.[70] For medical devices with limited surface area, e.g., on a vascular stent, the LbL contains several microgram selenium in total which would be equal to only a small fraction of normal dietary intake. At the same time, for larger devices, we are currently exploring the use of more stable organoselenium species which are catalytically active in RSNO decomposition. Indeed, it is known that aromatic RSe molecules are more stable than their aliphatic counterparts[62] and efforts to synthesize and utilize these species in preparation of NO generating LbL are currently in progress in this laboratory. By utilizing more stable forms of selenium catalyst, we also expect the resulting LbL can preserve more activity in long-term reaction period. It is likely that with reduced catalyst leaching and deactivation, the LbL methodology demonstrated here will be an attractive method to improve the thromboresistance of a wide range of blood contacting biomedical devices.

Supplementary Material

Refer to Web version on PubMed Central for supplementary material.

Acknowledgments

This work was supported by the National Institutes of Health (EB-004527). We gratefully thank Dr. Alvaro P. Rojas and Dr. Liandi Lou in Extracorporeal Membrane Oxygenation Laboratory at the University of Michigan Medical School for providing sheep blood used in this work, and Dr. Kai Sun and Dr. Haiping Sun in the University of Michigan Electron Microbeam Analysis Laboratory for their knowledgeable assistance in surface characterization.

Reference

1. Ratner, BD.; Hoffman, AS.; Schoen, FJ.; Lemons, JE. Biomaterials Science: An Introduction to Materials in Medicine. 2nd ed.. Elsevier Academic Press; 2004.
2. Ratner BD. Biomaterials 2007;28(34):5144–5147. [PubMed: 17689608]
3. Hodgson JM, Stone GW, Lincoff AM, Klein L, Walpole H, Bottner R, Weiner BH, Leon MB, Feldman T, Babb J, Dehmer GJ. Catheter. Cardiovasc. Interv 2007;69(3):327–333. [PubMed: 17219373]
4. Boos CJ, Lip GYH. Front. Biosci 2006;11:328–336. [PubMed: 16146734]
5. Bailly AL, Lautier A, Laurent A, Guiffant G, Dufaux J, Houdart E, Labarre D, Merland JJ. Int. J. Artif. Organs 1999;22(10):690–700. [PubMed: 10585134]
6. Bertrand OF, Sipehia R, Mongrain R, Rodes JR, Tardif JC, Bilodeau L, Cote G, Bourassa MG. J. Am. Coll. Cardiol 1998;32(3):562–571. [PubMed: 9741494]
7. Gorbet MB, Sefton MV. Biomaterials 2004;25(26):5681–5703. [PubMed: 15147815]
8. Ma SC, Meyerhoff ME. Mikrochim. Acta 1990;1(3–4):197–208.
9. Mowery KA, Schoenfisch MH, Saavedra JE, Keefer LK, Meyerhoff ME. Biomaterials 2000;21(1):9–21. [PubMed: 10619674]
10. Skrzypchak AM, Lafayette NG, Bartlett RH, Zhou ZR, Frost MC, Meyerhoff ME, Reynolds MM, Annich GM. Perfusion-Uk 2007;22(3):193–200.
11. Wu YD, Rojas AP, Griffith GW, Skrzypchak AM, Lafayette N, Bartlett RH, Meyerhoff ME. Sens. Actuators, B 2007;121(1):36–46.
12. Wu YD, Zhou ZR, Meyerhoff ME. J. Biomed. Mater. Res., Part A 2007;81A(4):956–963.
13. Cheung PY, Salas E, Schulz R, Radomski MW. Semin. Perinatol 1997;21(5):409–417. [PubMed: 9352613]
14. Davie EW, Fujikawa K, Kisiel W. Biochemistry 1991;30(43):10363–10370. [PubMed: 1931959]
15. Gladwin MT, Schechter AN, Kim-Shapiro DB, Patel RP, Hogg N, Shiva S, Cannon RO, Kelm M, Wink DA, Espey MG, Oldfield EH, Pluta RM, Freeman BA, Lancaster JR, Feelisch M, Lundberg JO. Nat. Chem. Biol 2005;1(6):308–314. [PubMed: 16408064]
16. Luscher TF, Barton M. Clin. Cardiol 1997;20(11):3–10. [PubMed: 8994730]
17. McRea JC, Kim SW. Trans. Am. Soc. Artif. Intern. Organs 1978;24:746–752. [PubMed: 362677]
18. Michiels C. J. Cell. Physiol 2003;196(3):430–443. [PubMed: 12891700]
19. Moncada S, Mullane KM, Vane JR. Br. J. Pharmacol 1979;66(1):P96–P97.
20. Olsson P, Sanchez J, Mollnes TE, Riesenfeld J. J. Biomater. Sci., Polym. Ed 2000;11(11):1261–1273. [PubMed: 11263812]
21. Batchelor MM, Reoma SL, Fleser PS, Nuthakki VK, Callahan RE, Shanley CJ, Politis JK, Elmore J, Merz SI, Meyerhoff ME. J. Med. Chem 2003;46(24):5153–5161. [PubMed: 14613318]
22. Wu B, Gerlitz B, Grinnell BW, Meyerhoff ME. Biomaterials 2007;28(28):4047–4055. [PubMed: 17597201]
23. Zhou ZR, Meyerhoff ME. Biomaterials 2005;26(33):6506–6517. [PubMed: 15941584]
24. Zhou ZR, Annich GM, Wu YD, Meyerhoff ME. Biomacromolecules 2006;7(9):2565–2574. [PubMed: 16961319]
25. Frost MC, Reynolds MM, Meyerhoff ME. Biomaterials 2005;26(14):1685–1693. [PubMed: 15576142]

26. Reynolds MM, Frost MC, Meyerhoff ME. Free Radic. Biol. Med 2004;37(7):926–936. [PubMed: 15336308]
27. Taite LJ, Yang P, Jun HW, West JL. J. Biomed. Mater. Res., Part B 2008;84B(1):108–116.
28. DeRosa F, Kibbe MR, Najjar SF, Citro ML, Keefer LK, Hrabie JA. J. Am. Chem. Soc 2007;129(13): 3786–3787. [PubMed: 17343382]
29. Reynolds MM, Hrabie JA, Oh BK, Politis JK, Citro ML, Keefer LK, Meyerhoff ME. Biomacromolecules 2006;7(3):987–994. [PubMed: 16529441]
30. Cha W, Meyerhoff ME. Biomaterials 2007;28(1):19–27. [PubMed: 16959311]
31. Cha W, Meyerhoff ME. Langmuir 2006;22(25):10830–10836. [PubMed: 17129067]
32. Bertrand P, Jonas A, Laschewsky A, Legras R. Macromol. Rapid Commun 2000;21(7):319–348.
33. Decher G, Eckle M, Schmitt J, Struth B. Curr. Opin. Colloid Interface Sci 1998;3(1):32–39.
34. Decher G. Science 1997;277(5330):1232–1237.
35. Fendler JH. Chem. Mater 1996;8(8):1616–1624.
36. Yu DG, Lin WC, Lin CH, Yeh YH, Yang MC. J. Biomed. Mater. Res., Part B 2007;83B(1):105–113.
37. Chen W, McCarthy TJ. Macromolecules 1997;30(1):78–86.
38. Levasalmi JM, McCarthy TJ. Macromolecules 1997;30(6):1752–1757.
39. Phuvanartnuruks V, McCarthy TJ. Macromolecules 1998;31(6):1906–1914.
40. Hsieh MC, Farris RJ, McCarthy TJ. Macromolecules 1997;30(26):8453–8458.
41. Lappan U, Buchhammer HM, Lunkwitz K. Polymer 1999;40(14):4087–4091.
42. Park J, Hammond PT. Macromolecules 2005;38(25):10542–10550.
43. Delcorte A, Bertrand P, Wischerhoff E, Laschewsky A. Langmuir 1997;13(19):5125–5136.
44. Moby V, Boura C, Kerdjoudj H, Voegel JC, Marchal L, Dumas D, Schaaf P, Stoltz JF, Menu P. Biomacromolecules 2007;8(7):2156–2160. [PubMed: 17585807]
45. Huang LY, Yang MC. J. Nanosci. Nanotechnol 2006;6(9–10):3163–3170. [PubMed: 17048532]
46. Ji JA, Tan QG, Fan DZ, Sun FY, Barbosa MA, Shen JC. Colloids Surf., B 2004;34(3):185–190.
47. Tan QG, Ji J, Barbosa MA, Fonseca C, Shen JC. Biomaterials 2003;24(25):4699–4705. [PubMed: 12951013]
48. Elbert DL, Herbert CB, Hubbell JA. Langmuir 1999;15(16):5355–5362.
49. Ciferri, A. Supramolecular Polymers. Marcel Dekker Inc; New York: 2000. p. 531
50. Jacob C, Maret W, Vallee BL. Proc. Natl. Acad. Sci. U. S. A 1999;96(5):1910–1914. [PubMed: 10051568]
51. Haughland, RP. Handbook of Fluorescent Probes and Research Chemicals. 6th ed.. Spence, MTZ., editor. Molecular Probes; OR: 1996.
52. http://www.sigmaaldrich.com/sigma/product%20information%20sheet/f4274pis.pdf
53. Williams DLH. Acc. Chem. Res 1999;32(10):869–876.
54. Yang SG, Zhang YJ, Zhang XY, Guan Y, Xu J, Zhang XL. ChemPhysChem 2007;8(3):418–424. [PubMed: 17183526]
55. Jiang XM, Chen ZC, Lv DS, Wu Q, Lin XF. Macromol. Chem. Phys 2008;209(2):175–183.
56. Garza JM, Schaaf P, Muller S, Ball V, Stoltz JF, Voegel JC, Lavalle P. Langmuir 2004;20(17):7298–7302. [PubMed: 15301518]
57. Lavalle P, Gergely C, Cuisinier FJG, Decher G, Schaaf P, Voegel JC, Picart C. Macromolecules 2002;35(11):4458–4465.
58. Ostrander JW, Mamedov AA, Kotov NA. J. Am. Chem. Soc 2001;123(6):1101–1110. [PubMed: 11456663]
59. Dejeu J, Buisson L, Guth MC, Roidor C, Membrey F, Charraut D, Foissy A. Colloids Surf., A 2006;288(1–3):26–35.
60. Crea F, Crea P, De Robertis A, Sammartano S. J. Chem. Eng. Data 2007;52(1):279–285.
61. Wong PSY, Hyun J, Fukuto JM, Shirota FN, DeMaster EG, Shoeman DW, Nagasawa HT. Biochemistry 1998;37(16):5362–5371. [PubMed: 9548918]
62. Painter EP. Chem. Rev 1941;28(2):179–213.

63. Ursini F, Heim S, Kiess M, Maiorino M, Roveri A, Wissing J, Flohe L. Science 1999;285(5432): 1393–1396. [PubMed: 10464096]

64. Whanger P, Vendeland S, Park YC, Xia YM. Ann. Clin. Lab. Sci 1996;26(2):99–113. [PubMed: 8852418]

65. Wu SH, Oldfield JE, Whanger PD, Weswig PH. Biol. Reprod 1973;8(5):625–629. [PubMed: 4736545]

66. Klayman, DL. Organic selenium compounds: their chemistry and biology. Wiley-Interscience; New York: 1973.

67. Fleser PS, Nuthakki VK, Malinzak LE, Callahan RE, Seymour ML, Reynolds MM, Merz SI, Meyerhoff ME, Bendick PJ, Zelenock GB, Shanley CJ. J. Vasc. Surg 2004;40(4):803–811. [PubMed: 15472611]

68. Frost MC, Meyerhoff ME. J. Biomed. Mater. Res., Part A 2005;72A(4):409–419.

69. Frost MC, Rudich SM, Zhang HP, Maraschio MA, Meyerhoff ME. Anal. Chem 2003;75(4):1037–1037.

70. Rayman MP. Proc. Nutr. Soc 2002;61(2):203–215. [PubMed: 12133202]

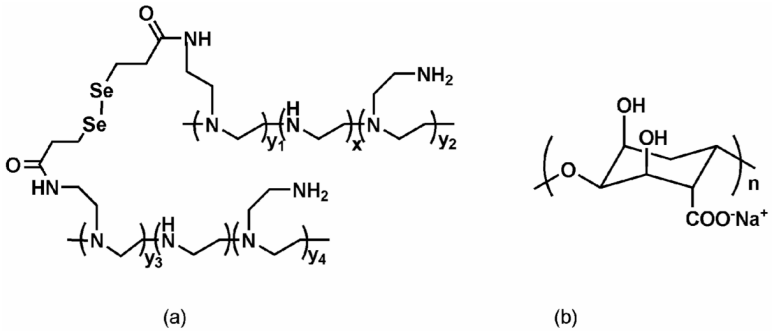

Figure 1.
Chemical structures of (a) organoselenium immobilized polyethyleneimine (SePEI) and (b) sodium alginate (Alg).

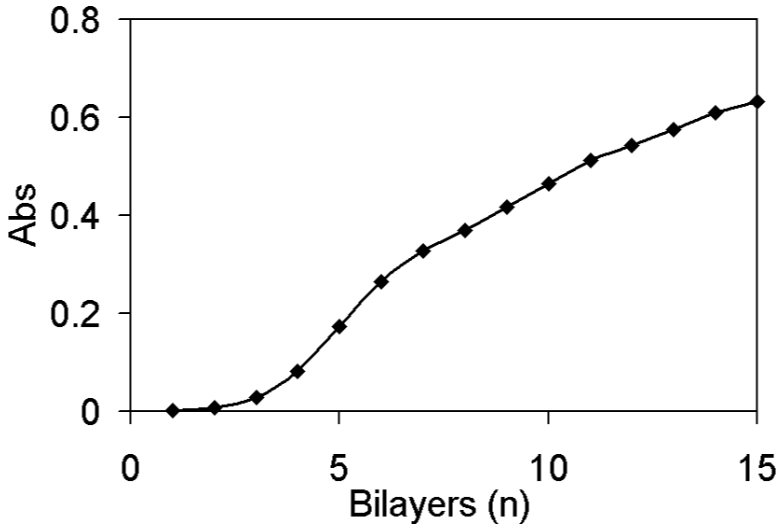

Figure 2.
Absorbance at 503 nm of $(SePEI/Alg)_n$ after every bilayer assembled.

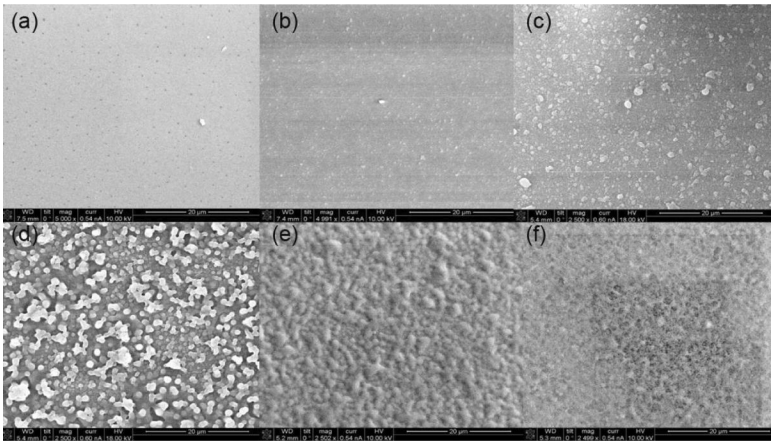

Figure 3.
SEM of $(SePEI/Alg)_n$ on quartz slide: (a) $(PDDA/Alg)_2$ precursor layer; (b) $(SePEI/Alg)_1$; (d) $(SePEI/Alg)_2$; (d) $(SePEI/Alg)_3$; (e) $(SePEI/Alg)_4$; (f) $(SePEI/Alg)_5$.

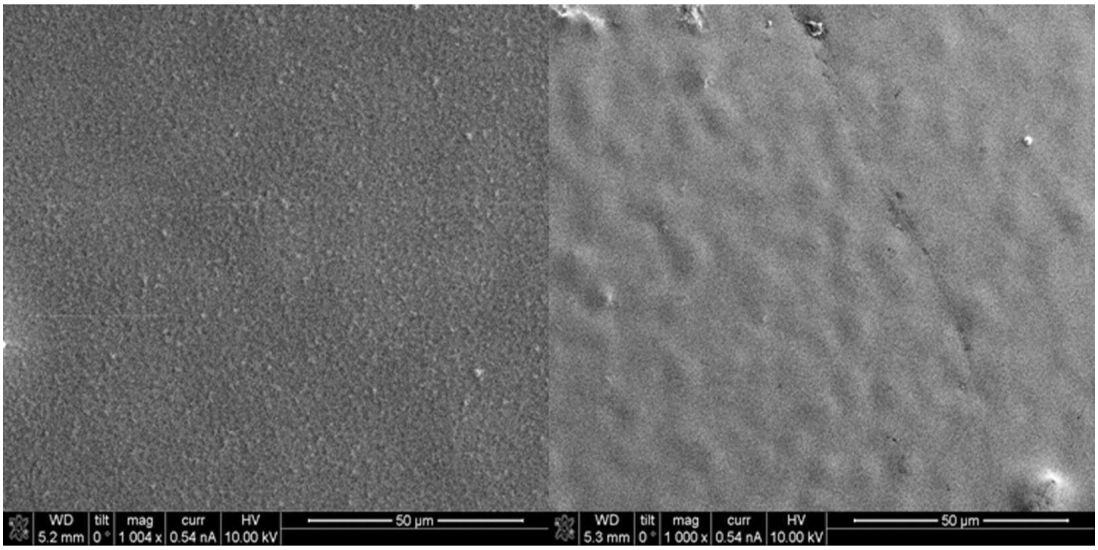

Figure 4.
SEM of a (SePEI/Alg)5 coated on quartz slide before (left) and after (after) annealed in PBS containing 100 μM GSH. Please note the pictures were taken at lower magnification than Figure 3.

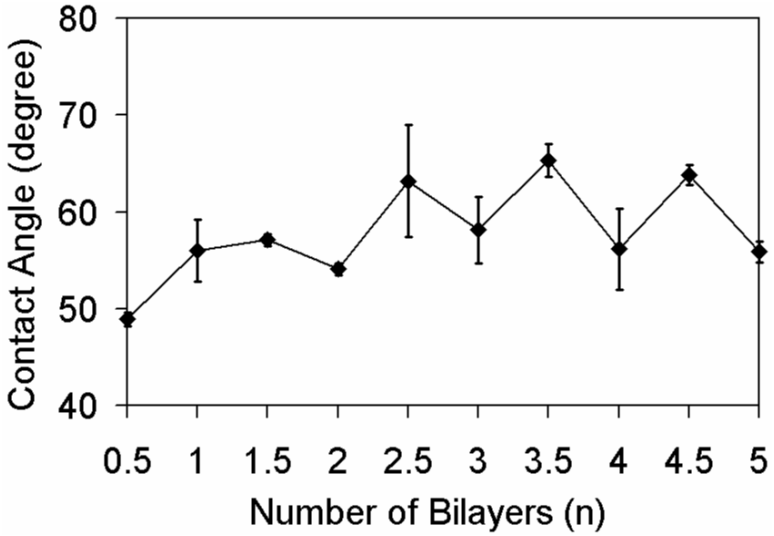

Figure 5.
Contact angles measured from films of a different number of adsorbed layers of polyelectrolytes. Integral numbers represent films with Alg as the outmost layer; otherwise, SePEI as the outmost layer.

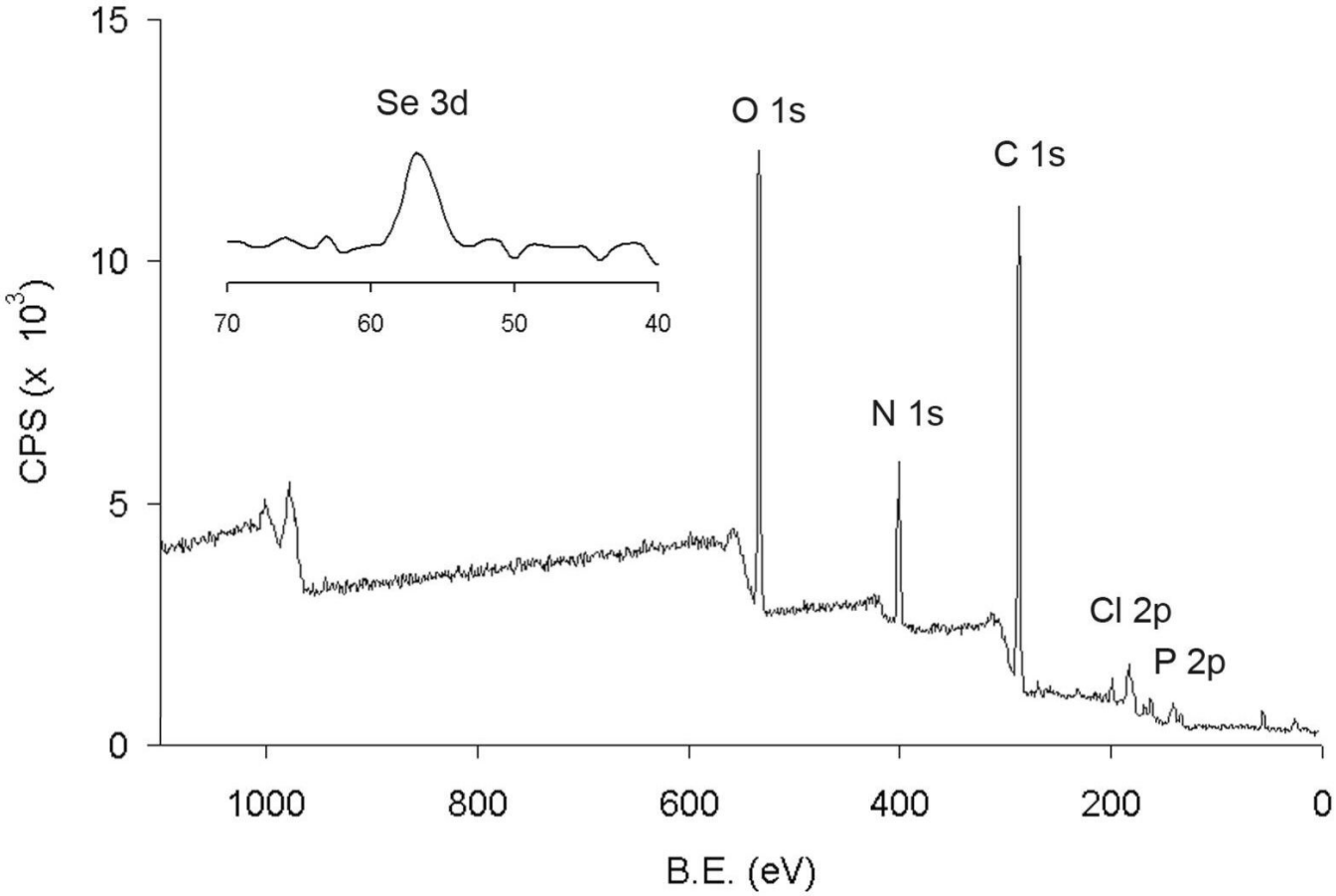

	C	N	O	Se	P	Cl
A%	62.41	13.90	21.42	0.94	0.88	1.46

Figure 6.
X-ray photoelectron spectroscopy of $(SePEI/Alg)_{15}$ on quartz substrate.

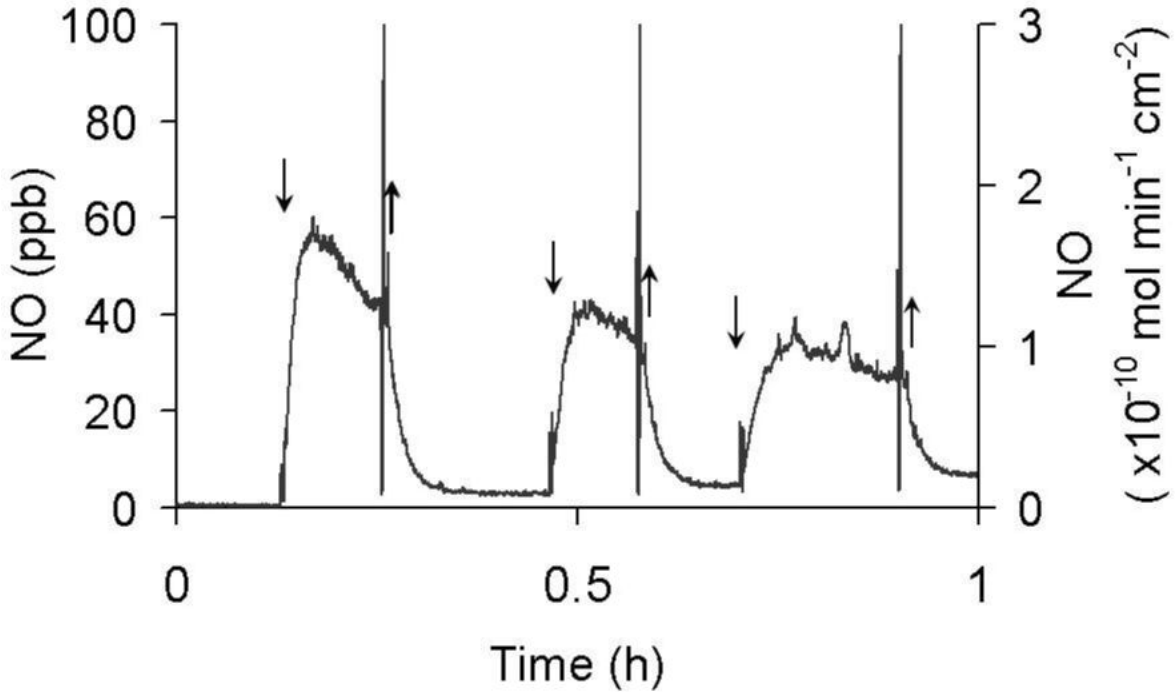

Figure 7.
NOA of $(SePEI/Alg)_5$ on quartz slide in PBS containing 50 μM GSNO, 50 μM GSH and 0.1 mM EDTA. The slide was immersed (↓)/removed (↑) as indicated by the arrows.

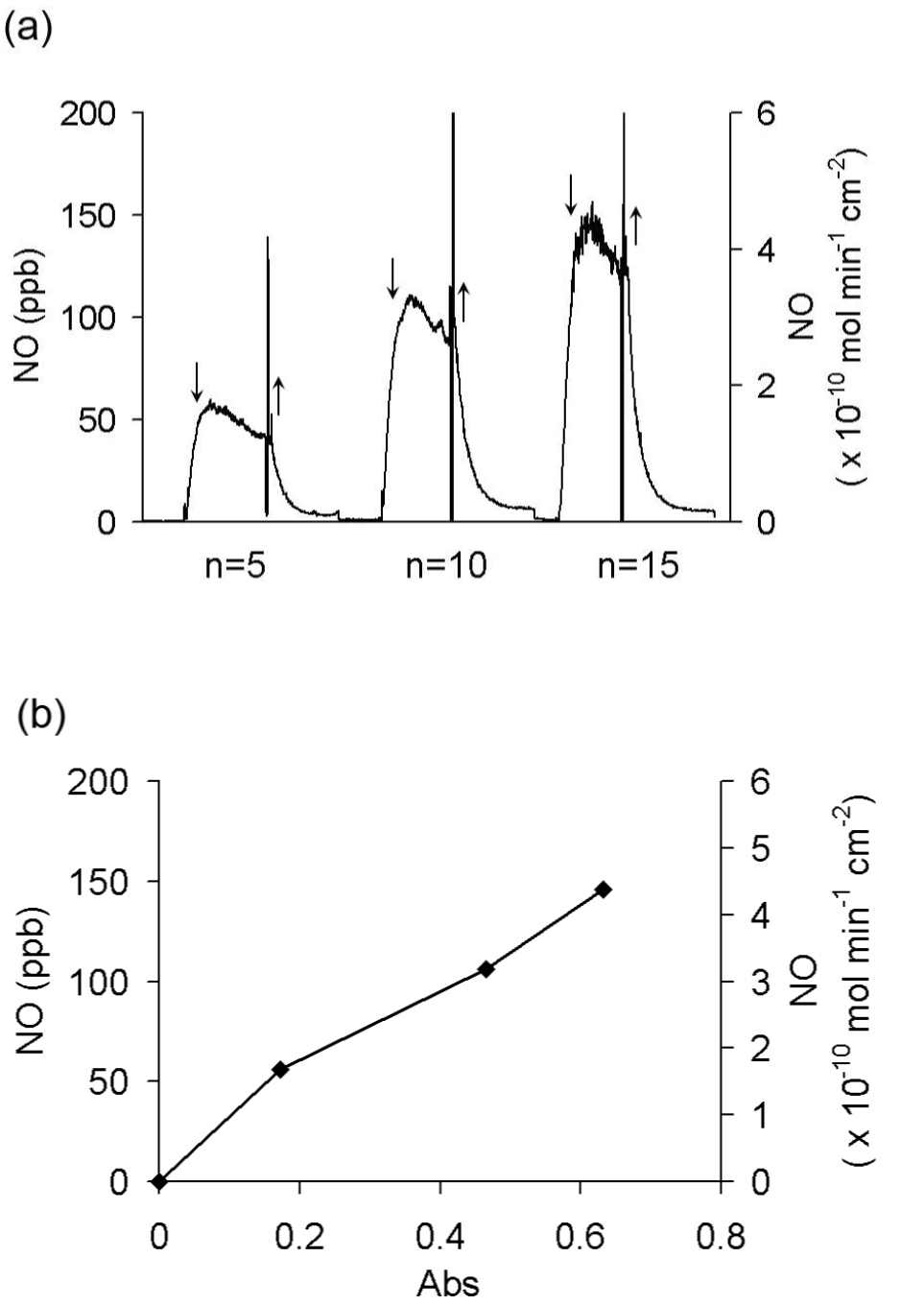

Figure 8.

(a) NO generation by $(SePEI/Alg)_n$ on quartz with various number of bilayers in PBS containing 50 μM GSNO, 50 μM GSH and 0.1 mM EDTA. The slide was immersed (↓)/ removed (↑) as indicated by the arrows. (b) NO flux vs. UV-Vis absorbance of $(SePEI/Alg)_n$ at 503 nm.

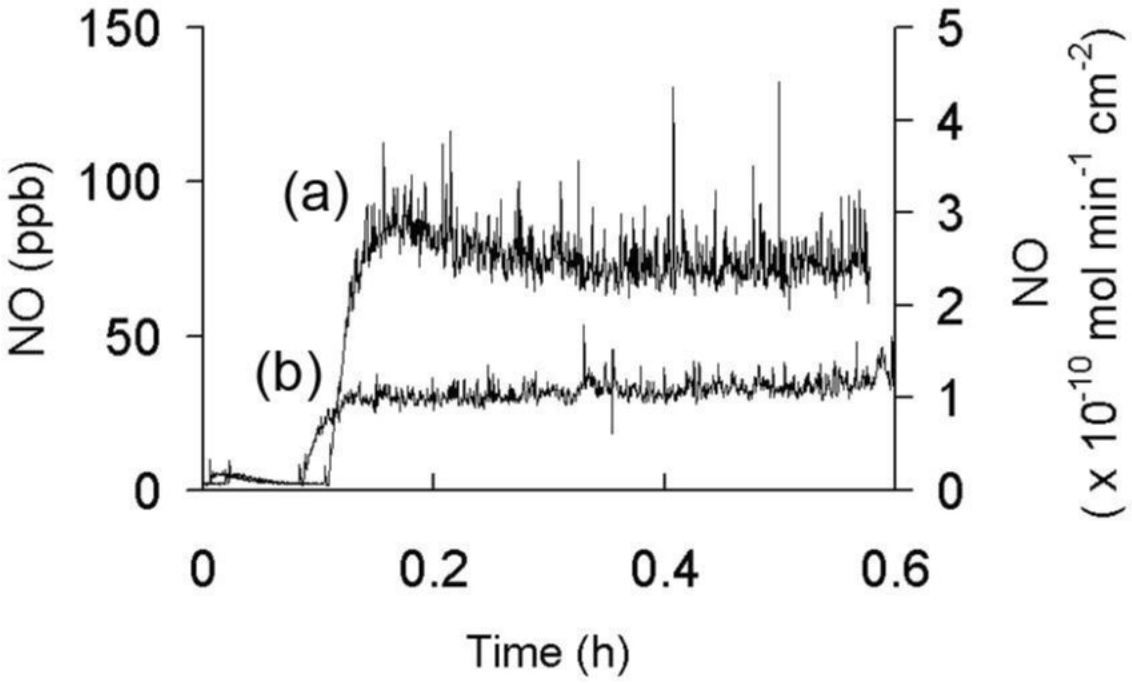

Figure 9.
NOA of $(SePEI/Alg)_{10}$ after 24 h incubation in (a) PBS; (b) sheep whole blood. Please note that both measurements were stopped before the added GSNO was depleted. The NOA curves here represent the average NO generation rate rather than total amount of NO produced.

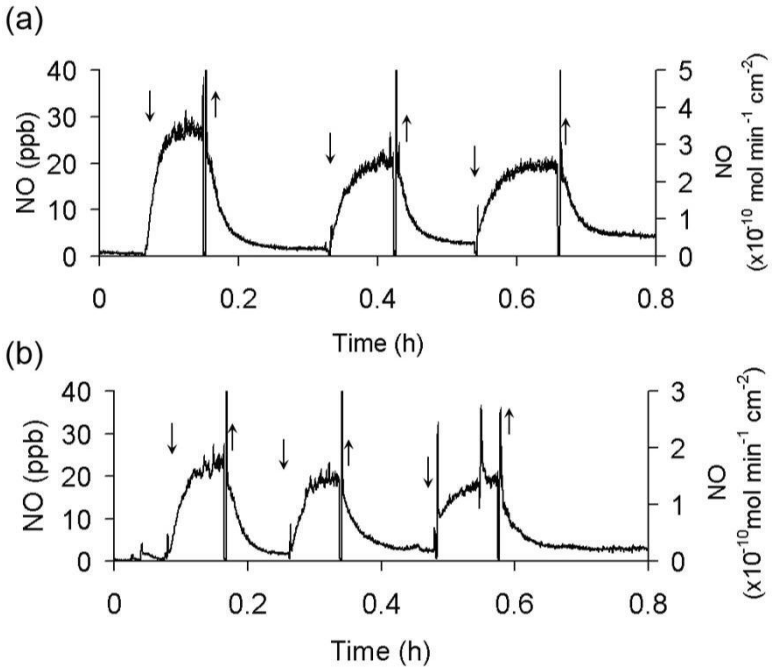

Figure 10.

NOA of (a) $(SePEI/Alg)_{10}$ on silicone rubber tubing; (b) $(SePEI/Alg)_{10}$ on PU catheter without application of $(PDDA/Alg)_2$ precursor layer. The segment of polyurethane catheter or silicone rubber tubing was immersed (↓)/removed (↑) as indicated by the arrows.

$$\text{RSe-SeR} + \text{GSH} \rightleftharpoons \text{RSe-SG} + \text{RSe}^- + \text{H}^+ \quad (1)$$

$$\text{RSe-SG} + \text{GSH} \rightleftharpoons \text{RSe}^- + \text{H}^+ + \text{GS-SG} \quad (2)$$

$$\text{RSe}^- + \text{H}^+ + \text{R'S-NO} \rightleftharpoons {}^1/_2\text{RSe-SeR} + \text{R'SH} + \text{NO} \quad (3)$$

$$\text{RSe-SeR} + 2\text{R'S-NO} \rightleftharpoons 2\text{RSe-SR'} + 2\text{NO} \quad (4)$$

Scheme 1.

Proposed RSNO decomposition mechanism by organoselenium catalyst using glutathione (GSH) as reducing agent. Each species represents: RSe-SeR, diselenide; GSH, thiol; RSe^-, selenolate; RSe-SG and RSe-SR', selenosulfide; GS-SG, disulfide; R'S-NO, S-nitrosothiol.